



Ex vivo fluorescence confocal microscopy: prostatic and periprostatic tissues atlas and evaluation of the learning curve

Laura Bertoni¹ · Stefano Puliatti^{2,3} · Luca Reggiani Bonetti⁴ · Antonino Maiorana⁴ · Ahmed Eissa^{2,5}  · Paola Azzoni¹ · Luigi Bevilacqua² · Valentina Spandri² · Shaniko Kaleci¹ · Ahmed Zoeir^{2,5} · Maria Chiara Sighinolfi² · Salvatore Micali² · Giampaolo Bianchi² · Giovanni Pellacani⁶ · Bernardo Rocco² · Rodolfo Montironi⁷

Received: 6 September 2019 / Revised: 17 December 2019 / Accepted: 22 December 2019

© Springer-Verlag GmbH Germany, part of Springer Nature 2020

Abstract

Ex vivo fluorescence confocal microscopy (FCM) is an optical technology that provides fast H&E-like images of freshly excised tissues, and it has been mainly used for “real-time” pathological examination of dermatological malignancies. It has also shown to be a promising tool for fast pathological examination of prostatic tissues. We aim to create an atlas for FCM images of prostatic and periprostatic tissues to facilitate the interpretation of these images. Furthermore, we aimed to evaluate the learning curve of images interpretation of this new technology. Eighty fresh and unprepared biopsies obtained from radical prostatectomy specimens were evaluated using the FCM VivaScope® 2500 M-G4 (Mavig GmbH, Munich, Germany; Caliber I.D.; Rochester NY, USA) by two pathologists. Images of FCM with the corresponding H&E are illustrated to create the atlas. Furthermore, the two pathologists were asked to re-evaluate the 80 specimens after 90 days interval in order to assess the learning curve of images’ interpretation of FCM. FCM was able to differentiate between different types of prostatic and periprostatic tissues including benign prostatic glands, benign prostatic hyperplasia, high-grade intraepithelial neoplasm, and prostatic adenocarcinoma. As regards the learning curve, FCM demonstrated a short learning curve. We created an atlas that can serve as the base for urologists and pathologists for learning and interpreting FCM images of prostatic and periprostatic tissues. Furthermore, FCM images is easily interpretable; however, further studies are required to explore the potential applications of this new technology in prostate cancer diagnosis and management.

Keywords Fluorescence confocal microscope · Prostate cancer · Atlas · Learning curve

Laura Bertoni and Stefano Puliatti contributed equally to this work.

Electronic supplementary material The online version of this article (<https://doi.org/10.1007/s00428-019-02738-y>) contains supplementary material, which is available to authorized users.

✉ Stefano Puliatti
stefanopuliatti@gmail.com

¹ Department of Surgical, Medical, Dental and Morphological Sciences with Interest transplant, Oncological and Regenerative Medicine, University of Modena and Reggio Emilia, Modena, Italy

² Department of Urology, University of Modena and Reggio Emilia, Modena, Italy

³ Department of Urology, Ospedale Policlinico e Nuovo Ospedale Civile S. Agostino Estense Modena, University of Modena and Reggio Emilia, Via del Pozzo, 71, 41124 Modena, Italy

⁴ Department of Pathology, Ospedale Policlinico e Nuovo Ospedale Civile S. Agostino Estense Modena, University of Modena and Reggio Emilia, Modena, Italy

⁵ Urology Department, Faculty of Medicine, Tanta University, Tanta, Egypt

⁶ Department of Dermatology, University of Modena and Reggio Emilia, Modena, Italy

⁷ Department of Pathological Anatomy, Polytechnic University of the Marche Region, School of Medicine, United Hospitals, Ancona, Italy

Introduction

Ex vivo fluorescence confocal microscopy (FCM) is a novel optical technology that allows the examination of freshly excised tissue to provide a quasi-histological view of the tissues in few minutes. FCM is based on the combination of two types of lasers to allow the examination of tissue specimens using the reflectance mode (785 nm) that depends on the difference of the refractive indices of various cellular structure, and the fluorescence mode (488 nm) that utilizes a contrast agent to allow the visualization of microstructures [20].

To date, FCM has been used in healthy skin [12] as well as in cutaneous lesions such as melanoma [10, 11], basal cell carcinoma, and squamous cell carcinoma [9, 17]. Furthermore, it was used for diagnosis of cutaneous inflammatory skin lesions [3]. Moreover, Ragazzi M et al. [26] examined the use of FCM on different surgical specimens such as breast, lymph node, thyroid, and colon, demonstrating that neoplastic tissues were easily distinguishable from normal structures.

The main advantage of the FCM is its ability to provide quasi-histological images that are similar to hematoxylin and eosin (H&E) images, which render the interpretation of images easier for pathologist novice to this technology.

Prostate cancer (PCa) is predicted to be the most commonly diagnosed male cancer in the USA in 2019 [29]. The gold standard diagnosis of PCa is based on the histopathological examination of prostatic tissues. Infiltrative growth pattern, absence of basal cell layer, and nuclear atypia (nuclear enlargement and prominent nuclei) represent the main pathological criteria for PCa diagnosis [19]. However, histopathological examination of tissues is a time-consuming procedure that may require up to 2 days in the highest quality pathological laboratories [1]. Currently, there is an increased interest in “real-time” pathological examination of prostatic tissues either during prostate biopsies or during radical prostatectomy [28, 31]. In this setting, several options were introduced for “real time” pathological examination of prostatic and periprostatic tissues including frozen section [28], light reflectance spectroscopy [21], multiphoton microscopy [30], confocal laser endomicroscopy [18], video-rate fluorescence-structured illumination microscopy [32], and FCM [24].

The aim of the current study is to create an atlas for the FCM images demonstrating its ability to identify different architectural structures in prostatic specimens (such as muscle, nerves, vessels, and adipose tissue) with differentiation of inflammatory changes from malignant transformation. Furthermore, among the important factors, determining the feasibility and superiority of any new imaging technology is the accurate and easy interpretation of its images. This can be demonstrated by assessing the learning curve of this new technology [15]. Thus, the learning curve for FCM images interpretation was evaluated as a secondary aim.

Material and methods

Patients

This study was approved by the Ethical Committee (protocol number 0018091/18) and written informed consent was obtained from all patients. Clinical data and pathological features were anonymously stored. We evaluated 80 prostatic biopsies of 18 gauge in thickness, obtained from radical prostatectomy (RP) specimens of 10 consecutive patients with clinically localized PCa undergoing robotic-assisted laparoscopic prostatectomies (RALP) using Da Vinci Surgical System (Intuitive Surgical, Inc., Sunnyvale, CA, USA).

Specimens and staining procedure

The fresh, no formalin fixed, biopsies were obtained within 10 min from the removal of the prostate, and were separately stained in a 0.6 mM solution of acridine orange dye (Sigma-Aldrich®) for 30 s then washed in physiological saline solution. All biopsies were placed between two glass slides sealed with silicon glue and then positioned onto the FCM stage for image acquisition. Following the acquisition, the samples were covered with a thin sponge, poned in biocassettes, and immersed in 10% neutral buffered formalin for 24-h fixation in order to maintain the proper orientation of the samples at the further histopathological examination.

Instrument

The FCM VivaScope® 2500 M-G4 (Mavig GmbH, Munich, Germany; Caliber I.D.; Rochester NY, USA) has two different lasers. In this study, both reflectance (785 nm) and fluorescence (488 nm) modes were used for each sample examination. Briefly, FCM has maximum examination depth of 200 µm, a vertical resolution of up to 4 µm, a magnification of $\times 550$ and a maximum scan size of 25×25 mm [20]. However, the penetration depth can be increased by modifying the laser power and/or the incubation period of the specimen. Moreover, both sides of the glass slides can be examined by the FCM allowing deeper examination of the specimen. The reconstructed image is a collection of mosaic images (square-shaped images of 1024×1024 pixels). The laser filter has a $\times 38$, 0.85 numerical aperture water immersion objective lens. The softwares VivaScan® (Version 11.0.1140 Mavig GmbH; Caliber I.D), VivaBlock®, and VivaStack® enable respectively the reconstruction of the images from the probes, the acquisition of multiple images in the X/Y directions within a single plane at a fixed depth, and a survey of multiple frames along the Z axis, visualizing deeper tissue. The grayscale fluorescence and reflectance mosaics were digitally stained with color and combined. Since pathologists interpret hematoxylin and eosin (H&E) staining, the purple and pink colors were

used to improve association with cellular nuclei and non-cellular structures, respectively [8]. In this study, a self-written ImageJ software (<https://imagej.nih.gov/ij/>) was used to the standard digital image staining approach. Zoom capabilities enable an enhanced visualization of cell morphology details. The staining and imaging processes of each specimen were completed within 5 min.

FCM images' evaluation

All FCM images were stored in a dedicated database. Two pathologists (general pathologist and an expert genitourinologist) from two different centers (University of Modena and Reggio Emilia and University of Ancona) were integrated in the assessment of the FCM learning curve. The images were randomly displayed to each of the two pathologists while being blinded to the histopathologic diagnoses. After more than 90 days, they were asked to re-evaluate the specimens. All examinations were performed independently and included the evaluation of the tumor and non-neoplastic tissue comprised in the samples with particular regard to normal prostatic glands and soft tissue components (muscle bundles, nerve, adipocytes, vessels) as well as other non-neoplastic conditions such as inflammation and benign glandular hyperplasia.

Histopathological examination

From the biopsies included in paraffin and processed according to the standard protocol [27], we performed 3 consecutive sections of 3 μm thickness, starting from the most superficial portion without discarding material. The sections were H&E stained.

Diagnostic criteria for carcinoma included atypical acini arranged in one or more patterns of growth, combined with atypical cytologic findings including prominent nucleolus or pale enlarged and irregular nuclei, were useful criteria for cancer, particularly when small, irregular, abortive acini with primitive lumens and absence of basal layer were visible. The tumor grade groups were assessed according to International Society of Urological Pathology (ISUP) grading [6]. Immunohistochemical analysis included racemases/34betaE12 cytokeratin cocktail stain and were used for 8 specimens with suspicious small foci of cancer detected on H&E-stained slides.

H&E-stained slides were compared with the images obtained by FCM techniques in order to describe overlaps or discordant features.

Statistical analysis

The Cohen's kappa (κ) statistic was used to measure the agreement between histopathologic diagnoses and the FCM diagnosis for each pathologist in each reading. We selected κ

statistic as the measure of agreement as our variable of interest is binary. Kappa is a measure of this difference, standardized to lie on a -1 to 1 scale, where 1 is perfect agreement, 0 is exactly what would be expected by chance, and negative values indicate agreement less than chance, i.e., potential systematic disagreement between the observers [5].

The Cohen's kappa can be interpreted as following; ($\kappa < 0$) is less than chance agreement, ($\kappa = 0.01$ to 0.20) represents slight agreement, ($\kappa = 0.21$ to 0.40) is fair agreement, ($\kappa = 0.41$ to 0.60) is moderate agreement, ($\kappa = 0.61$ to 0.80) is substantial agreement, while, ($\kappa = 0.81$ to 0.99) is considered almost perfect agreement. The interpretation of reproducibility is marginal ($\kappa = 0.00$ to 0.40), good ($\kappa = 0.40$ to 0.75), and excellent ($\kappa > 0.75$) [7].

The process of deciding whether the numerical results quantifying hypothesized relationships between variables, are acceptable as a description of the data, is known as validation. We select k-Fold Cross-Validation, as it reduces the risk of errors induced by bias by utilizing the full-data set for training and for validation. In K Fold cross validation, the data is divided into k subsets. Now the holdout method is repeated k times, such that each time, one of the k subsets is used as the test set/validation set and the other $k-1$ subsets are put together to form a training set. The error estimation is averaged over all k trials to get total effectiveness of our model [13].

Results

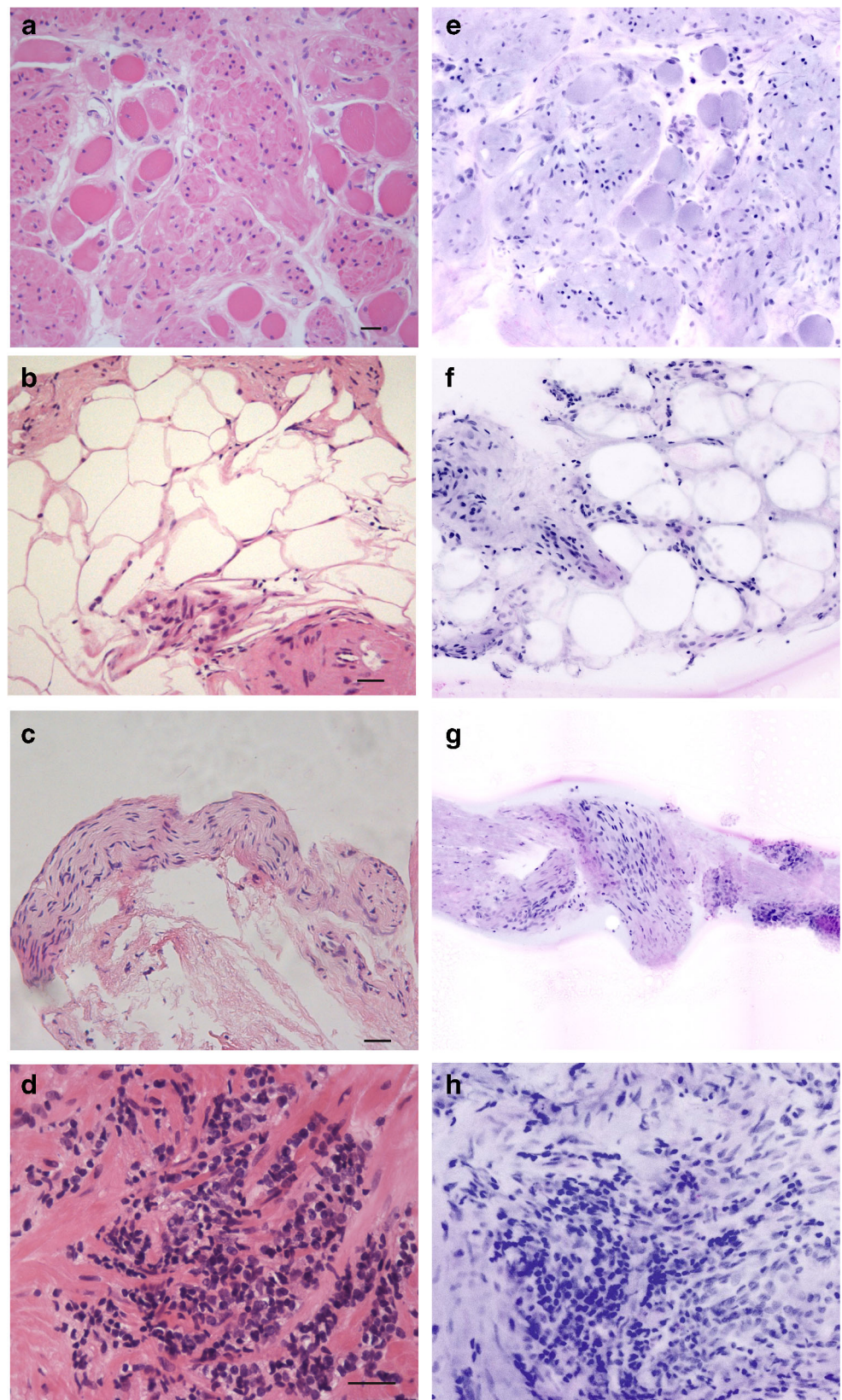
FCM atlas

Samples from the biopsies were classified as non-neoplastic tissue (NNT), high-grade prostatic intraepithelial neoplasia (HG-PIN), and prostatic acinar adenocarcinoma (PAA).

Non-neoplastic prostatic and extraprostatic tissues

In some samples, probably taken from the periphery of the prostatic gland, a mix of connective and soft adipose tissue, crossed by thin muscle bundles, were detected as well as bundles of nerves (Fig. 1a–c). Chronic prostatitis typically shows an aggregation of lymphocytes and plasma cells within the stroma (Fig. 1d). The different components of prostatic and periprostatic soft tissue were easily recognized at the corresponding FCM images (Fig. 1e–h). NNT included prostatic glands lined by typical two cell layers represented by an outer layer of low cuboidal cells and an inner layer of tall columnar mucin-secreting epithelium, organized into non-infiltrating pattern of growth. The glands are surrounded by a thin connective tissue and, sometimes, contained corpora amylacea (Fig. 2a, b). As shown in Fig. 2d, e, in FCM mosaics, different cell layers of the prostatic glands as well as corpora amylacea were appreciable. Hyperplastic prostatic glands with taller and

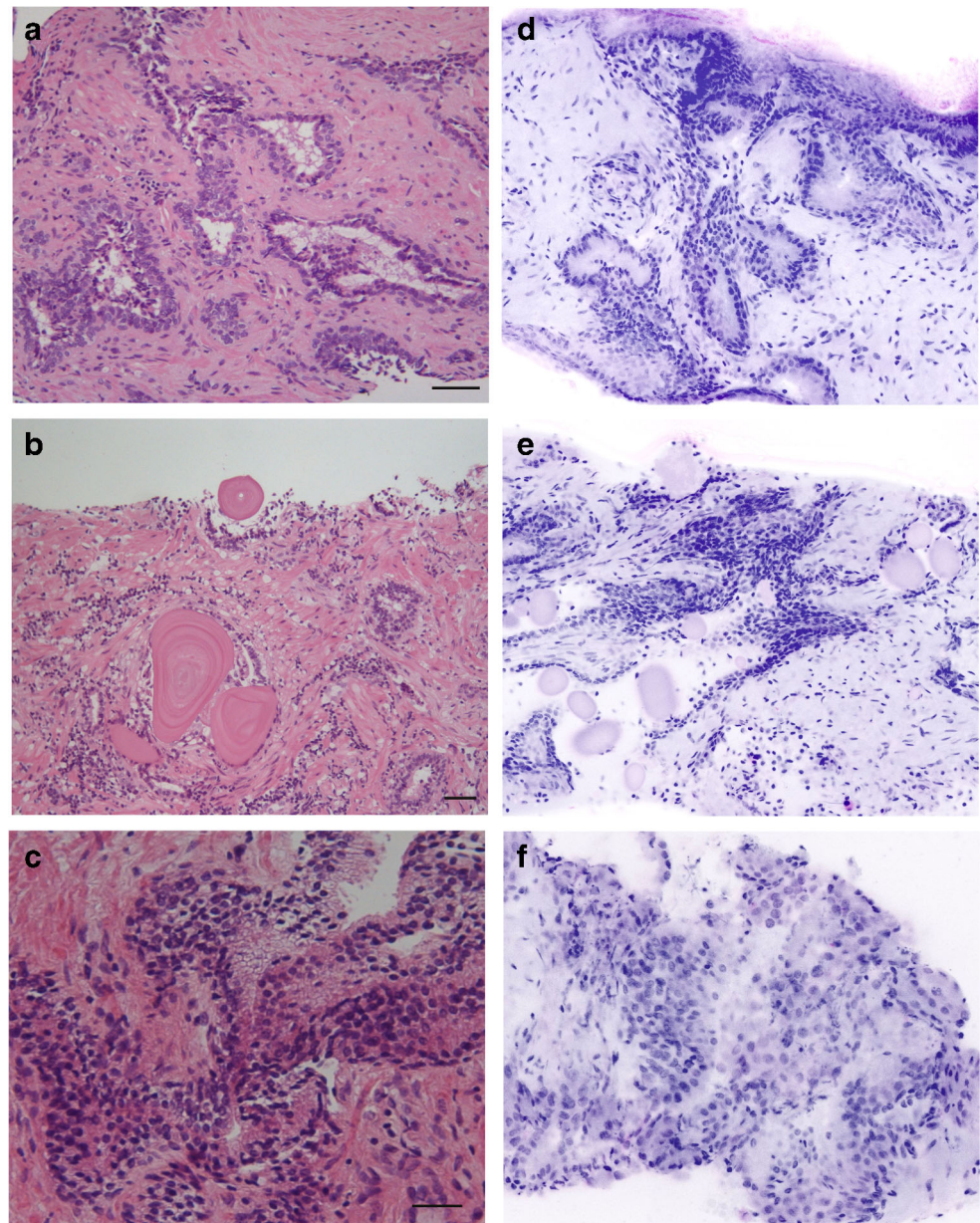
Fig. 1 Histological images of non-neoplastic extraprostatic muscle bundles (**a**), adipose tissue (**b**), nerve (**c**) and prostatic inflammatory infiltrate (**d**), and FCM correlates (**e–h**). (Scale bar, 100 μ m)



enlarged columnar secretory cells, with pale to clear cytoplasm and enlarged nuclei without atypia, are

visible in the samples. The glands are evidently surrounded by basal cells (Fig. 2c, f).

Fig. 2 Histological images of prostatic glands (a), corpora amylacea (b) and hyperplastic prostatic glands (c), and FCM corresponding images (d–f). (Scale bar, 100 μ m)



High-grade prostatic intraepithelial neoplasia and prostatic acinar adenocarcinoma

HG-PIN included glands composed of crowded and irregularly spaced multi-layered epithelial cells, with enlarged, hyperchromatic and pleomorphic nuclei, with prominent nucleoli. Basal cells surrounded the glands (Fig. 3a). At FCM, we observed the prominent nucleolus and the stratified epithelium surrounded by evident basal cells (Fig. 3e).

PAA was composed of closely packed irregular glands variably in size and shape and with back-to-back distribution. Few or no interposing stroma was intermingled through the atypical glands. Enlarged round, hyperchromatic nuclei and prominent nucleolus are visible. Basal cells were absent.

These tumors were graduated as grade group 1 [GG1] (Fig. 3b). Tumor composed by predominantly well-formed glands and exhibiting a lesser component of cribriform glands were classified as grade group 2 [GG2] (Fig. 3c); whereas the cribriform glands were predominant; the tumors were classified as grade group 3 [GG3]. When sheet of undifferentiated cell and poorly formed/fused glands were detected, we classified the tumors as grade group 4 [GG4] (Fig. 3d). The corresponding FCM images demonstrated the atypia of the nuclei, the irregular morphology of the glands, as well as the typical pattern of growth of the glands (Fig. 3f–h). Figure 4 a and b emphasize the infiltrating growth of PAA within a nerve and the atypia of the glands with particular regard among the prominent nucleolus and the absence of the basal cell layer. These features

Fig. 3 Histological images and the corresponding FCM images of high-grade prostatic intraepithelial neoplasia (**a–e**) and prostatic acinar adenocarcinoma grade group 1 (**b–f**), grade group 2 (**c–g**), and grade group 3 (**d–h**). (Scale bar, 100 μ m)

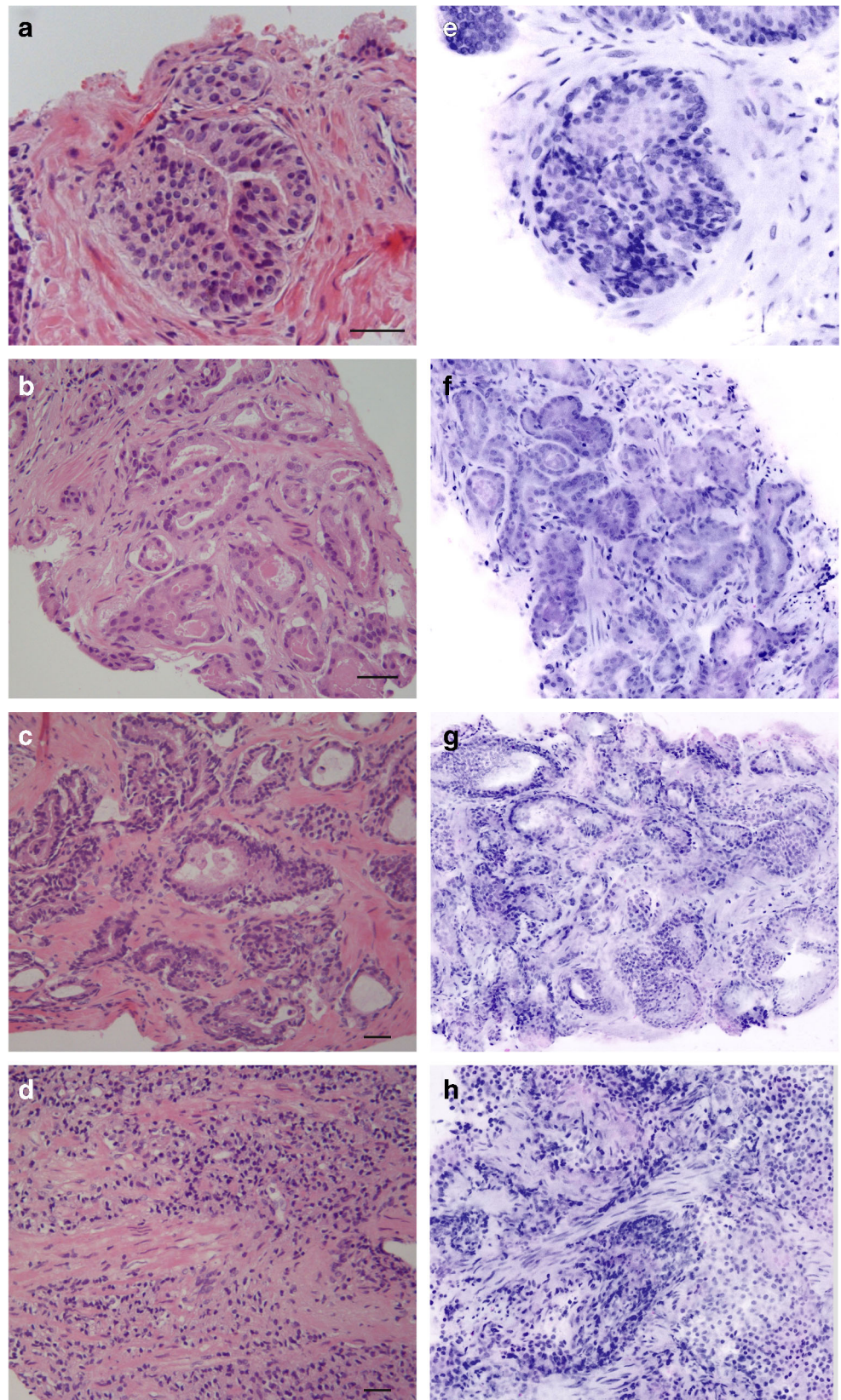
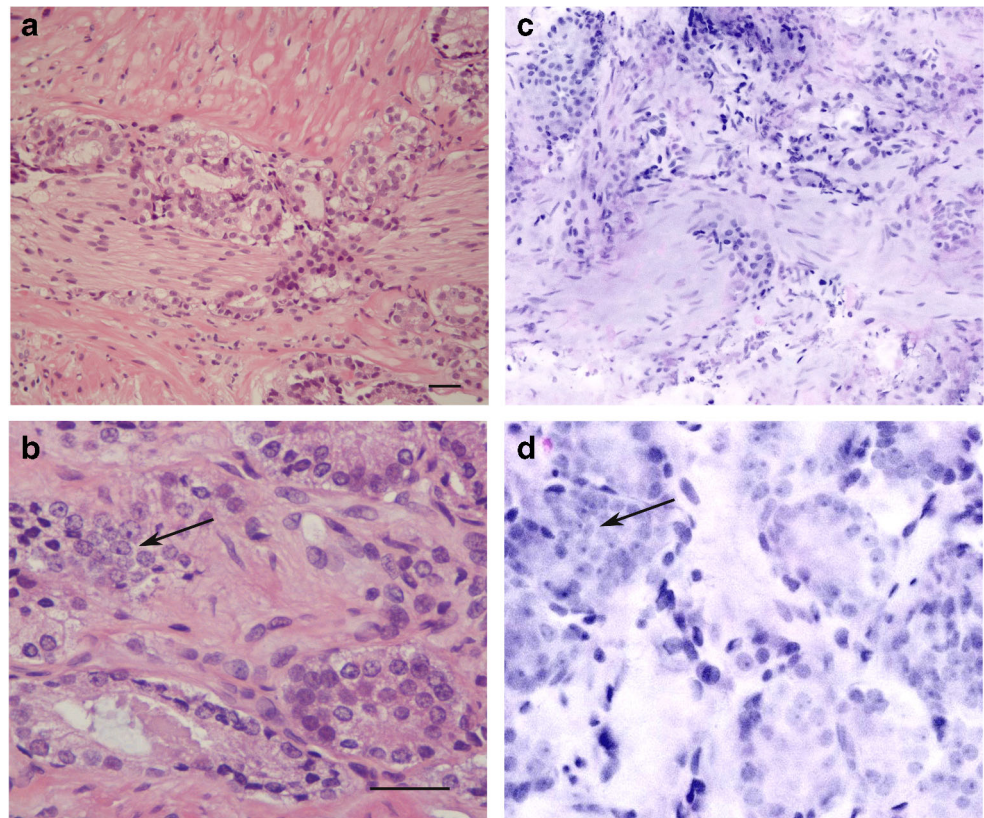


Fig. 4 Histological images and FCM correlates of infiltrating growth of PAA within a nerve (a–c) and atypical glands with prominent nucleolus and the absence of the basal cell layer (b–d). (Scale bar, 50 μ m)



were well represented by the corresponding FCM images (Fig. 4c, d).

Learning curve assessment

Both pathologists achieved very encouraging levels of agreement between FCM evaluation and the gold standard histopathological diagnosis of prostatic biopsies (Table 1). The percentages of agreement become higher from the first evaluation 86% and 92% ($\kappa = 0.68$ and $\kappa = 0.79$ substantial agreement) to the second one, reaching 95% ($\kappa = 0.87$ almost

perfect agreement) for both the pathologists. Furthermore, the reproducibility was excellent ($\kappa > 0.75$) for both raters in the second evaluation. Besides high accuracy, Table 1 also indicates a promising result in terms of specificity and sensitivity. Out of 59 negative biopsies, 50 and 57 have been correctly identified as negative by the first pathologist in the first (specificity 84.7%) and second evaluations (specificity 96.6%), respectively. For the second pathologist, 58 negative biopsies have been correctly identified both in the first and the second evaluations which correspond to 98.3% specificity. On the other hand, 19/21 positive biopsies have been correctly

Table 1 First and second FCM evaluation of prostatic biopsies compared to histopathological diagnoses, the percentage of correct diagnoses, κ value, the level of agreement, the sensitivity, the specificity, and ROC area for both raters

			Histopathological diagnoses		% of correct diagnosis	κ value	Level of agreement	Sensitivity	Specificity	ROC area
			Negative	Positive						
FCM evaluation	Rater 1	Negative	50	2	86%	0.68	Substantial	90%	85%	0.87
	First evaluation	Positive	9	19						
	Rater 1	Negative	57	2	95%	0.87	Almost perfect	90%	97%	0.93
	Second evaluation	Positive	2	19						
	Rater 2	Negative	58	5	92%	0.79	Substantial	76%	98%	0.87
	First evaluation	Positive	1	16						
	Rater 2	Negative	58	3	95%	0.87	Almost perfect	86%	98%	0.92
	Second evaluation	Positive	1	18						

classified by the first pathologist in both evaluations which leads to a sensitivity value of 90.5%. The second pathologist correctly identified 16/21 positive samples during the first evaluation and 18/21 in the second evaluation (sensitivity 76.2% and 85.7% respectively). Moreover, the area under the receiver operating characteristic (ROC) curve, that describes the relationship between the sensitivity and specificity, becomes higher from the first to the second evaluation (from 0.87 to 0.92–0.93, respectively) for both raters.

Discussion

Surgeons show growing interest in the real-time pathological examination as it may potentially allow a more precise and patient-tailored surgery [25]. In PCa, real-time pathological examination plays an important role as it may be used for assessing the surgical margins (apical, bladder neck, and neurovascular bundle) during radical prostatectomy thus allowing complete resection of the tumor without compromising the functional outcomes [18, 22, 30]. It can be also used during prostate biopsy to decrease the need for additional biopsies [31]. Furthermore, it has been used in the histopathological screening for prostate cancer in organ donors, especially with the increasing age of organ donors [2]. The gold standard technique for real-time pathological examination is the frozen section, which, is debatable due to its associated drawbacks including the technical difficulty, the complexity of the procedure that requires multiple dedicated personnel, and being resource and time-consuming technique [22]. Other options include light reflectance spectroscopy [21], multiphoton microscopy [30], confocal laser endomicroscopy [18], and video-rate fluorescence structured illumination microscopy [32]. Furthermore, we have previously proved that FCM has a diagnostic accuracy of 91% compared to the standard histopathological examination with AUC, sensitivity, and specificity of 0.884, 83.33%, and 93.53% for the pathological examination of prostatic tissues [24], which render FCM as a promising option for “real-time” pathological examination of prostatic tissue.

In the current study, FCM was able to provide a rapid, and high-resolution quasi histological images of the freshly excised, non-formalin fixed prostatic and periprostatic specimens. The primary aim of our study was to create an atlas for the FCM images for prostatic and periprostatic tissue examination; however, throughout the process of collecting representative images for the atlas, FCM demonstrated a promising results in identifying cellular and nuclear characters of prostatic and periprostatic tissues with almost perfect agreement ($\kappa = 0.87$) compared to the gold standard histopathological examination after a short learning curve. Furthermore, it was able to accurately differentiate benign tissues and

inflammatory changes from malignant transformation in the prostatic specimens.

However, we did not assess the potentiality of FCM to assess the specimens grade group; FCM was able to identify the tumor growth pattern of specimens used for creating this atlas. Currently, we have an ongoing study that will assess the ability of FCM to identify the group grade.

The learning curve is among the most important limitations of any new technology. It is important to examine the learning curve of image interpretation before any new cellular imaging technology is introduced in the clinical practice [14, 16]. In these setting, we evaluated the learning curve of FCM images. We intentionally integrated a general pathologist and an expert genitourinary pathologist in the evaluation of the learning curve to provide a more realistic assessment. We hypothesized that the great similarity between the FCM images and the gold standard H&E histopathological examination will render them easily interpretable by pathologists novice to FCM. Our results supported this hypothesis, since the agreement between the FCM reading and the histopathological diagnosis increased from 86 to 92% in the first reading for the first and the second pathologists, respectively, to reach 95% for both pathologists in the second reading. Noteworthy, 8 samples (10%) required immunohistochemistry for diagnosis, which, may be responsible for the persistent 5% disagreement obtained by both pathologists on the second reading. Interestingly, Bertoni et al. [4] demonstrated that FCM is capable of providing immunofluorescent images of special markers using fluorochrome-conjugated antibodies, which may enhance the diagnostic performance of FCM of doubtful cases; however, in their study, they used paraffin-fixed sections and not freshly excised specimens. Panarello D et al. [23] reported that the learning curve for the confocal laser endomicroscopy images interpretation seems to be short; however, this was not assessed in their study.

FCM provides several advantages including the H&E-like images which facilitate the interpretation of images, the fast preparation of specimens and rapid image acquisition (less than 5 min per specimen in our experience), and the preservation of the specimens’ integrity not only for subsequent histopathological examination but also for ancillary studies like immunohistochemistry [25]. Furthermore, FCM represents a step forward towards digitalized pathology, as the specimen preparation is simple and can be performed by the treating surgeon, and it provides a digital image that can be sent online to a remote pathologist for interpretation. Despite the promising level of agreement between FCM evaluation and the histopathological examination of prostatic and periprostatic tissues, there were some pitfalls (Supplementary Fig. 1); one of the specimens with prostatic acinar adenocarcinoma on the H&E was misdiagnosed as HG-PIN due to the presence of mild nuclear atypia associated with crowded nuclei in the FCM images. Moreover, adenocarcinoma cells were

misdiagnosed as a result of the presence of technical artefact that masqueraded mild atypia in another specimen. Finally, in one specimen, a focus of atypical grade group 4 single cells were misdiagnosed as inflammatory cells.

The main limitation of the current study is the small sample size. On the other hand, our study has many strengths as it is the first study (to our knowledge) to provide a comprehensive description of the FCM images of the prostatic and periprostatic tissue and to assess the learning curve of this technology in the field of PCa.

Conclusion

FCM is an optical technology that can be used for “real-time” pathological examination of prostatic tissue. This atlas can serve as the base for urologists and pathologists for learning and interpreting FCM images of prostatic and periprostatic tissues. Further studies are required to define the potential applications of FCM in PCa.

Authors Contributions Bertoni L., Puliatti S., Eissa A., Sighinolfi MC, Bianchi G, Pellacani G, Rocco B, Montironi R: Conception and Design. Bertoni L, Puliatti S, Regianni Bonetti L, Maiorana A, Azzoni P, Bevilacqua L, Spandri V, Montironi R: Acquisition of Data. Kaleci S: Data Analysis. Bertoni L, Puliatti S, Regianni Bonetti L, Maiorana A, Eissa A, Azzoni P, Sighinolfi MC, Micali S, Rocco B, Montironi R: Interpretation of Data. Bertoni L, Puliatti S, Regianni Bonetti L, Eissa A, Zoeir A, Sighinolfi MC: Drafting and writing. Micali S, Bianchi G, Pellacani G, Rocco B, Montironi R: Revision

Compliance with ethical standards

This study was approved by the Ethical Committee in the university of Modena & Reggio Emilia (protocol number 0018091/18) and written informed consent was obtained from all patients.

Conflict of interest Eissa A has a temporary contract of consultation with MAVIG GmbH.

References

- Alshieban S, Al-Surimi K (2015) Reducing turnaround time of surgical pathology reports in pathology and laboratory medicine departments. *BMJ Qual Imp Rep* 4:u209223–w203773. <https://doi.org/10.1136/bmjquality.u209223.w3773>
- Avellini C, Baccarani U, Orsaria M, Adani GL, Bresadola V, Lorenzin D, Bresadola F, Beltrami CA (2009) Evaluation of prostate cancer staging in organ donors: intraoperative histology on periglandular soft tissues—a proposal. *Transplant Proc* 41:1099–1103. <https://doi.org/10.1016/j.transproceed.2009.03.089>
- Bertoni L, Azzoni P, Reggiani C, Pisciotta A, Carnevale G, Chester J, Kaleci S, Reggiani Bonetti L, Cesinaro AM, Longo C, Pellacani G (2018) Ex vivo fluorescence confocal microscopy for intraoperative, real-time diagnosis of cutaneous inflammatory diseases: a preliminary study. *Exp Dermatol* 27:1152–1159. <https://doi.org/10.1111/exd.13754>
- Bertoni L, Pisciotta A, Azzoni P, Bertani G, Reggiani Bonetti L, Puliatti S, Farnetani F, Carnevale G, Pellacani G (2018) Use of ex vivo fluorescence confocal microscopy for detection of tissue specific markers. *Biomed J Sci & Tech Res* 10. <https://doi.org/10.26717/BJSTR.2018.10.002003>
- Edgar B (2004) Applied nonparametric statistical methods. P. Sprent and N. C. Smeeton, Chapman & Hall/CRC, London, England, 2001. No. of pages: ix+461. Price:£29.99. ISBN: 1-584-88145-3 Statistics in medicine 23:1988-1989. <https://doi.org/10.1002/sim.1755>
- Epstein JI, Egevad L, Amin MB, Delahunt B, Srigley JR, Humphrey PA (2016) The 2014 International Society of Urological Pathology (ISUP) Consensus Conference on Gleason Grading of Prostatic Carcinoma: definition of grading patterns and proposal for a new grading system. *Am J Surg Pathol* 40: 244–252. <https://doi.org/10.1097/pas.0000000000000530>
- Fleiss JL (1981) The measurement of interrater agreement. *Statistical Methods for Rates and Proportions*, 2nd Edition. Edn. Wiley, New York, pp 212–236
- Gareau DS, Li Y, Huang B, Eastman Z, Nehal KS, Rajadhyaksha M (2008) Confocal mosaicing microscopy in Mohs skin excisions: feasibility of rapid surgical pathology. *J Biomed Opt* 13:054001. <https://doi.org/10.1117/1.2981828>
- Hartmann D, Krammer S, Bachmann MR, Mathemeier L, Ruzicka T, Bagci IS, von Braunmuhl T (2018) Ex vivo confocal microscopy features of cutaneous squamous cell carcinoma. *J Biophotonics* 11: e201700318. <https://doi.org/10.1002/jbio.201700318>
- Hartmann D, Krammer S, Ruini C, Ruzicka T, von Braunmuhl T (2016) Correlation of histological and ex-vivo confocal tumor thickness in malignant melanoma. *Lasers Med Sci* 31:921–927. <https://doi.org/10.1007/s10103-016-1936-5>
- Hartmann D, Krammer S, Vural S, Bachmann MR, Ruini C, Sardy M, Ruzicka T, Berking C, von Braunmuhl T (2018) Immunofluorescence and confocal microscopy for ex-vivo diagnosis of melanocytic and non-melanocytic skin tumors: a pilot study. *J Biophotonics* 11. <https://doi.org/10.1002/jbio.201700211>
- Hartmann D, Ruini C, Mathemeier L, Dietrich A, Ruzicka T, von Braunmuhl T (2016) Identification of ex-vivo confocal scanning microscopic features and their histological correlates in human skin. *J Biophotonics* 9:376–387. <https://doi.org/10.1002/jbio.201500124>
- Hastie T, Tibshirani R, Friedman J (2009) The elements of statistical learning data mining, inference, and prediction. Springer Verlag, Secaucus
- Jain M, Pulijal SV, Rajadhyaksha M, Halpern AC, Gonzalez S (2018) Evaluation of bedside diagnostic accuracy, learning curve, and challenges for a novice reflectance confocal microscopy reader for skin cancer detection in vivo. *JAMA Derm* 154:962–965. <https://doi.org/10.1001/jamadermatol.2018.1668>
- Kuiper T, Kiesslich R, Ponsioen C, Fockens P, Dekker E (2012) The learning curve, accuracy, and interobserver agreement of endoscope-based confocal laser endomicroscopy for the differentiation of colorectal lesions. *Gastrointest Endosc* 75:1211–1217. <https://doi.org/10.1016/j.gie.2012.01.040>
- Liu J, Li M, Li Z, Zuo XL, Li CQ, Dong YY, Zhou CJ, Li YQ (2014) Learning curve and interobserver agreement of confocal laser endomicroscopy for detecting precancerous or early-stage esophageal squamous cancer. *PLoS One* 9:e99089. <https://doi.org/10.1371/journal.pone.0099089>
- Longo C, Borsari S, Pampena R, Benati E, Bombonato C, Raucci M, Mirra M, Di Stefani A, Peris K, Pellacani G (2018) Basal cell carcinoma: the utility of in vivo and ex vivo confocal microscopy. *J Eur Acad Dermatol Venereol* 32:2090–2096. <https://doi.org/10.1111/jdv.14984>
- Lopez A, Zlatev DV, Mach KE, Bui D, Liu JJ, Rouse RV, Harris T, Leppert JT, Liao JC (2016) Intraoperative optical biopsy during robotic assisted radical prostatectomy using confocal

- endomicroscopy. *J Urol* 195:1110–1117. <https://doi.org/10.1016/j.juro.2015.10.182>
19. Magi-Galluzzi C (2018) Prostate cancer: diagnostic criteria and role of immunohistochemistry *Modern pathology : an official journal of the United States and Canadian. Acad Pathol, Inc* 31:S12–S21. <https://doi.org/10.1038/modpathol.2017.139>
 20. MAVIG (2018) Datasheet VivaScope® 2500M-G4 https://www.vivascope.de/wp-content/uploads/2019/06/DS_VS-2500M-G4_287_0219-ohne-Mohs.pdf. Accessed 4 January 2020
 21. Morgan MS, Lay AH, Wang X, Kapur P, Ozayar A, Sayah M, Zeng L, Liu H, Roehrborn CG, Cadeddu JA (2016) Light reflectance spectroscopy to detect positive surgical margins on prostate cancer specimens. *J Urol* 195:479–483. <https://doi.org/10.1016/j.juro.2015.05.115>
 22. Obek C, Saglican Y, Ince U, Argun OB, Tuna MB, Doganca T, Tufek I, Keskin S, Kural AR (2018) Intra-surgical total and reconstructible pathological prostate examination for safer margins and nerve preservation (Istanbul preserve). *Ann Diagn Pathol* 33: 35–39. <https://doi.org/10.1016/j.anndiagpath.2017.11.010>
 23. Panarello D, Comperat E, Seyde O, Colau A, Terrone C, Guillonnet B (2019) Atlas of ex vivo prostate tissue and cancer images using confocal laser endomicroscopy: a project for intraoperative positive surgical margin detection during radical prostatectomy. *Eur Urol Focus*. <https://doi.org/10.1016/j.euf.2019.01.004>
 24. Puliatti S, Bertoni L, Pirola GM, Azzoni P, Bevilacqua L, Eissa A, Elsherbiny A, Sighinolfi MC, Chester J, Rocco B, Micali S, Bagni I, Reggiani Bonetti L, Maiorana A, Malvey J, Longo C, Montironi R, Bianchi G, Pellacani G (2019) Ex-vivo fluorescence confocal microscopy: the first application for real-time pathologic examination of prostatic tissue. *BJU Int*. <https://doi.org/10.1111/bju.14754>
 25. Ragazzi M, Longo C, Piana S (2016) Ex vivo (fluorescence) confocal microscopy in surgical pathology: state of the art. *Adv Anat Pathol* 23: 159–169. <https://doi.org/10.1097/pap.0000000000000114>
 26. Ragazzi M, Piana S, Longo C, Castagnetti F, Foroni M, Ferrari G, Gardini G, Pellacani G (2014) Fluorescence confocal microscopy for pathologists *Modern pathology : an official journal of the United States and Canadian. Acad Pathol, Inc* 27:460–471. <https://doi.org/10.1038/modpathol.2013.158>
 27. Samaratunga H, Montironi R, True L, Epstein JI, Griffiths DF, Humphrey PA, van der Kwast T, Wheeler TM, Srigley JR, Delahunt B, Egevad L (2011) International Society of Urological Pathology (ISUP) consensus conference on handling and staging of radical prostatectomy specimens. Working group 1: specimen handling *Modern pathology : an official journal of the United States and Canadian. Acad Pathol, Inc* 24:6–15. <https://doi.org/10.1038/modpathol.2010.178>
 28. Schlomm T, Tennstedt P, Huxhold C, Steuber T, Salomon G, Michl U, Heinzer H, Hansen J, Budaus L, Steurer S, Wittmer C, Minner S, Haese A, Sauter G, Graefen M, Huland H (2012) Neurovascular structure-adjacent frozen-section examination (NeuroSAFE) increases nerve-sparing frequency and reduces positive surgical margins in open and robot-assisted laparoscopic radical prostatectomy: experience after 11,069 consecutive patients. *Eur Urol* 62:333–340. <https://doi.org/10.1016/j.eururo.2012.04.057>
 29. Siegel RL, Miller KD, Jemal A (2019) Cancer statistics, 2019 *CA Cancer J Clin* 69:7–34. doi: <https://doi.org/10.3322/caac.21551>
 30. Tewari AK, Shevchuk MM, Sterling J, Grover S, Herman M, Yadav R, Mudalair K, Srivastava A, Rubin MA, Zipfel WR, Maxfield FR, Xu C, Webb WW, Mukherjee S (2011) Multiphoton microscopy for structure identification in human prostate and periprostatic tissue: implications in prostate cancer surgery. *BJU Int* 108:1421–1429. <https://doi.org/10.1111/j.1464-410X.2011.10169.x>
 31. Wang M, Kimbrell HZ, Sholl AB, Tulman DB, Elfer KN, Schlichenmeyer TC, Lee BR, Lacey M, Brown JQ (2015) High-resolution rapid diagnostic imaging of whole prostate biopsies using video-rate fluorescence structured illumination microscopy. *Cancer Res* 75:4032–4041. <https://doi.org/10.1158/0008-5472.can-14-3806>
 32. Wang M, Tulman DB, Sholl AB, Kimbrell HZ, Mandava SH, Elfer KN, Luethy S, Maddox MM, Lai W, Lee BR, Brown JQ (2016) Gigapixel surface imaging of radical prostatectomy specimens for comprehensive detection of cancer-positive surgical margins using structured illumination microscopy. *Sci Rep* 6:27419. <https://doi.org/10.1038/srep27419>

Publisher's note Springer Nature remains neutral with regard to jurisdictional claims in published maps and institutional affiliations.